The effect of presence and location of microcalcifications on atherosclerotic plaque rupture

A tissue-engineering approach

Crielaard, Hanneke; Jansen, Imke; van der Heiden, Kim; Kremers, Gert Jan; Gijsen, Frank J.H.; Farrell, Eric; Akyildiz, Ali C.

DOI
10.1016/j.jmbbm.2025.107139

Publication date
2025

Document Version
Final published version

Published in
Journal of the mechanical behavior of biomedical materials

Citation (APA)
Crielaard, H., Jansen, I., van der Heiden, K., Kremers, G. J., Gijsen, F. J. H., Farrell, E., & Akyildiz, A. C. (2025). The effect of presence and location of microcalcifications on atherosclerotic plaque rupture: A tissue-engineering approach. *Journal of the mechanical behavior of biomedical materials*, *171*, Article 107139. https://doi.org/10.1016/j.jmbbm.2025.107139

Journal of the Mechanical Behavior of Biomedical Materials 171 (2025) 107139

Contents lists available at ScienceDirect

Journal of the Mechanical Behavior of Biomedical Materials

journal homepage: www.elsevier.com/locate/jmbbm

The effect of presence and location of microcalcifications on atherosclerotic plaque rupture: A tissue-engineering approach

Hanneke Crielaard [a,1], Imke Jansen [a,1], Kim van der Heiden [a], Gert-Jan Kremers [d], Frank J.H. Gijsen [a,b], Eric Farrell [c], Ali C. Akyildiz [a,b,*]

[a] Department of Cardiology, Biomedical Engineering, Cardiovascular Institute, Thorax Center, Erasmus MC, University Medical Center Rotterdam, Rotterdam, the Netherlands
[b] Department of Biomechanical Engineering, Delft University of Technology, Delft, the Netherlands
[c] Department of Oral and Maxillofacial Surgery, Erasmus MC, University Medical Center Rotterdam, Rotterdam, the Netherlands
[d] Erasmus Optical Imaging Centre, Erasmus MC, University Medical Center Rotterdam, Rotterdam, the Netherlands

ARTICLE INFO

Keywords:
Atherosclerosis
Plaque rupture
Microcalcifications
Mechanics
Collagen
Tissue engineering

ABSTRACT

Rupture of the cap of an atherosclerotic plaque can trigger thrombotic cardiovascular events. It has been suggested, through computational models, that the presence and specific location of microcalcifications in the atherosclerotic cap can increase the risk of cap rupture. However, the experimental confirmation of this hypothesis is lacking. In this study, we investigated how the presence and location of microcalcifications, relative to the lumen, influence (local) mechanics and rupture behavior of atherosclerotic plaque caps.

Using tissue-engineered fibrous cap analogs with hydroxyapatite (HA) clusters to mimic calcifications in human plaque caps, we replicated the microcalcification distribution observed in human carotid plaques, as identified by our histological analysis. The analogs were imaged using multiphoton microscopy with second-harmonic generation to assess local collagen fiber orientation and dispersion. Subsequently, they underwent uniaxial tensile testing to failure, during which local strain and failure characteristics were analyzed.

Our results revealed that HA clusters, particularly those in the luminal region, contribute to increased local collagen fiber dispersion. Moreover, the presence of HA clusters reduced both failure tensile stress and strain in the TE cap analogs. Besides, the rupture location shifted toward the site of HA clusters. Additionally, rupture initiation was consistently found in high-strain regions, and in 86 % of the analogs, even at the highest strain location in the sample.

Our findings suggest that microcalcification clusters in plaque caps may increase the cap rupture risk and relocate the rupture site. Moreover, local strain measurements can serve as an additional tool for plaque cap rupture risk assessment.

1. Introduction

Approximately 60 % of cardiovascular events are triggered by the rupture of fibrous caps overlying lipid cores in atherosclerotic plaques in conduit arteries (Virmani et al., 2006). However, plaque rupture risk analysis is still not part of the clinical cardiovascular event risk assessment (Visseren et al., 2021). This is primarily due to the insufficient predictive power of the so-far proposed criteria for cap rupture risk, including the well-known geometric markers such as cap thickness (Jang et al., 2005) and lipid core size (Ohayon et al., 2008). Consequently, new cap-specific markers are needed to improve cap rupture risk assessment.

From a biomechanical viewpoint, fibrous cap rupture is a material failure, wherein the cap fails to sustain its integrity under applied mechanical forces and deformation (Kwak et al., 2014). Investigating the biomechanics of atherosclerotic cap rupture may reveal some long-awaited rupture risk markers. While the mechanical behavior of biological tissues is acknowledged to be determined by their underlying microstructure (Zadpoor, 2015), the mechanics of cap rupture and how

* Corresponding author. Department of Cardiology, Biomedical Engineering, Cardiovascular Institute, Thorax Center, Erasmus MC, University Medical Center Rotterdam, Ee2341, P.O. Box 2040, 3000 CA Rotterdam, the Netherlands.
E-mail address: a.akyildiz@erasmusmc.nl (A.C. Akyildiz).
[1] The authors Hanneke Crielaard and Imke Jansen contributed equally to the work.

https://doi.org/10.1016/j.jmbbm.2025.107139
Received 10 April 2025; Received in revised form 2 July 2025; Accepted 14 July 2025
Available online 16 July 2025

it is impacted by the underlying cap microstructure remain poorly understood.

Microcalcifications are abundant plaque components considered to play a critical role in cap rupture (Jansen et al., 2024). Microcalcifications are calcified particles, primarily composed of hydroxyapatite (HA), with a size typically not larger than 50 μm in diameter (Aikawa and et al., 2007; Moss and et al., 2020; New and Aikawa, 2013; Perrotta and Perri, 2017). Computational studies have suggested that individual microcalcifications affect cap stress and rupture risk (Bluestein and et al., 2008; Cilla et al., 2013; Corti and et al., 2022; Gijsen et al., 2021; Maldonado et al., 2015; Rambhia and et al., 2012; Vengrenyuk and et al., 2006; Wenk et al., 2010), by increasing cap stress levels (Aikawa and et al., 2007; Kelly-Arnold and et al., 2013; Vengrenyuk and et al., 2006) and/or relocating the peak cap stress (Cilla et al., 2013).

The computational models were based on simplified cap microstructures, assuming an isotropic and homogeneous matrix material in which the calcifications are embedded. This simplification overlooks the cap's heterogeneous, nonuniform, and anisotropic structural organization, including heterogeneity in collagen, which is known to impact plaque mechanics (Douglas et al., 2017; Johnston et al., 2021; Maldonado et al., 2015; Stöger and et al., 2012). Moreover, microcalcifications are often present in a plaque cap in clusters (Jansen et al., 2023), and not isolated, as modeled in computational studies. Also, the influence of the microcalcification cluster location on plaque rupture also remains unexplored. Therefore, systematic experimental studies are essential to validate computational findings and understand the influence of the presence and location of microcalcification clusters in the collagenous plaque cap to provide further insight into their effects on plaque rupture.

Although human plaque tissue from unruptured plaques has traditionally been the main source of experimental samples for studying plaque rupture (Cullen et al., 2003; Heiden et al., 2016), its scarcity impedes large-scale studies. To overcome this limitation, we previously developed a tissue-engineered (TE) plaque cap model of thin cap fibroatheroma (TCFA), which was shown as the plaque phenotype with the highest rupture risk (Wissing et al., 2022). The TE model consists of a collagenous tissue, mimicking the fibrous cap, with a collagen-poor inclusion, mechanically mimicking the plaque's lipid core. This model enables studies with varying structural composition to be conducted. Recently, we extended our cap model by incorporating HA clusters to mimic the microcalcifications in the caps (Jansen et al., 2023). In the current study, we use our TE cap model to experimentally investigate the impact of the presence and location, relative to the lumen, of microcalcification clusters on cap mechanics and rupture risk.

2. Methods

2.1. Localization of microcalcification clusters in human plaque caps

Human carotid plaque specimens were collected from seven patients undergoing carotid endarterectomy (CEA) at the Erasmus University Medical Center in Rotterdam, the Netherlands. The collection and usage of these samples were conducted in accordance with the Declaration of Helsinki and received approval from the hospital's Ethical Research Committee (MEC-2008-147). Histological cross-sections of 5 μm thickness (n = 90) were obtained. The localization of microcalcifications within these samples was assessed using Alizarin Red S staining. This analysis was conducted utilizing FIJI ImageJ software (US National Institutes of Health, Bethesda, MD, USA (Schindelin et al., 2012)). Microcalcification clusters were then categorized based on their location within the fibrous with respect to the lumen, either as a luminal cluster or as an abluminal cluster (located on the side of the lipid core). If microcalcification clusters showed no clear preference for either side, such as spreading over the entire cap or being located in the middle of the cap, they were excluded from categorization in either group.

2.2. Tissue-engineered cap analogs

2.2.1. Culture of MSCs

Human bone marrow mesenchymal stromal cells (MSCs) were utilized to develop the tissue-engineered cap analogs. These cells were isolated from iliac crest bone chips, which were collected from a paediatric patient (female) undergoing alveolar bone graft surgery. The collection was conducted with consent permitting the use of surgical waste material with an option for parental opt-out. This protocol received approval from the Medical Ethics Review Committee at Erasmus MC Medical Center Rotterdam, the Netherlands (MEC-2022-0163). The MSCs were expanded in αMEM (Gibco, Thermo Fisher Scientific, Breda, the Netherlands), supplemented with 10 % heat-inactivated fetal bovine serum (FBS, Sigma-Aldrich, St. Louis, USA), 50 μg/mL gentamycin, 1.5 μg/mL fungizone, 25 μg/mL L-ascorbic acid 2-phosphate (Sigma-Aldrich, St. Louis, USA) (base medium), supplemented with 1 ng/mL fibroblast growth factor-2 (Instruchemie B.V., Delfzijl, the Netherlands). The culturing was performed in a humidified incubator at 37 °C with 5 % CO2. Cells were expanded until they achieved 80 % confluency, at which point they were passaged for subsequent experimental setups up to passage 5.

2.2.2. TE cap culturing

Forty-three cap analogs were successfully cultured and were divided into three groups (Fig. 1): 1) Control group: no HA injection, 2) Luminal HA group: HA injection in the luminal side, and 3) Abluminal HA group: HA injection in the abluminal side. TE analogs from groups 2 and 3 were created so that the HA clusters would mimic the microcalcification clusters found in real plaques, based on the analysis of human carotid plaques (see the corresponding sections in the "Methodology" and "Results"). Throughout the manuscript, we refer to "HA clusters" specifically when discussing the TE cap analogs. In contrast, when referring to human plaque samples or drawing conclusions relevant to human pathology based on the TE caps, we use the term "microcalcifications." HA particles were introduced in clusters into the TE cap analogs of groups 2 and 3 to mechanically mimic microcalcifications within the fibrous cap, as described previously (Jansen et al., 2023). The amount and density of microcalcifications were previously suggested to significantly influence fibrous cap stresses (Corti et al., 2023; Wenk et al., 2010). Hence, we decided to model plaque caps with microcalcifications exclusively on either the abluminal or luminal side, rather than a combination of both, to ensure that the amount and density of HA clusters remained consistent across the analogs.

The TE cap analogs of the control group were created following the protocol described previously in detail (Crielaard et al., 2025; Jansen et al., 2023; Wissing et al., 2022). Briefly, MSCs ($1.5x10^6$ cells/ml) were seeded into 15 × 15 mm fibrin gels, a suspension of bovine fibrinogen (10 mg/ml, Sigma F8630) and bovine thrombin (10 U/ml, Sigma T4648) positioned between two Velcro strips. Fibrin served as a temporary, biocompatible scaffold that supports MSC viability and activity. During the first 7 days of culture, ε-Amino Caproic Acid (ε-ACA, 1 mg/ml, Sigma) was added to prevent premature fibrin break-down. To create the analogs with HA clusters (luminal and abluminal groups), a suspension of bovine fibrinogen (10 mg/ml) and HA microparticles (CAPTAL® 'R', Plasma Biotal Limited), 0.25 mg/ml) was prepared. Immediately after seeding MSCs into the fibrin gel between the Velcro strips, 5 μl clusters of the HA particle-fibrin suspension were injected using a pipette, just before the complete gelation of the MSC-fibrin gel. The analogs were then incubated for 30 min to allow gelation, after which culture medium was added.

For the luminal HA group, HA particles were first injected at one of the luminal sides of the analog and then at the other luminal side. By doing so, an HA cluster was created as close as possible to each luminal side. For the abluminal HA group, two injections of HA particles spaced approximately 5 mm apart were performed in the center of the analogs. This spacing was chosen to facilitate the creation of a soft inclusion (SI)

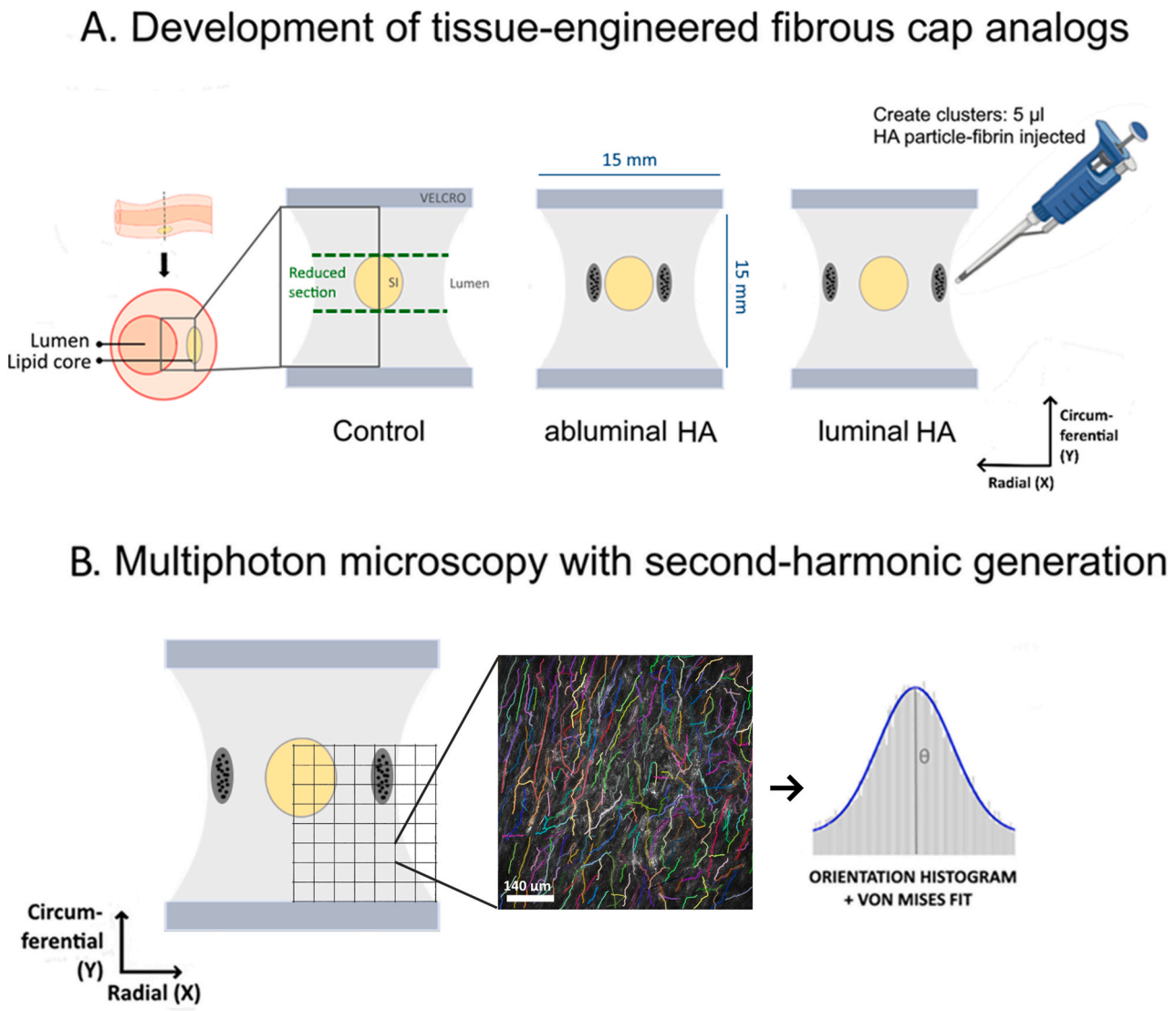

Fig. 1. Methodological pipeline of the study. A) Illustration depicting the simplified geometry of an atherosclerotic plaque cap (left) alongside the three groups of tissue-engineered cap analogs: Control, abluminal HA, and luminal HA. B) Collagen imaging with SHG-MPM and fiber orientation analysis. Scale bar = 140 µm C) Uniaxial tensile testing and DIC-derived local deformation measurements (SHG: second-harmonic generation, MPM: multiphoton microscopy, DIC: Digital image correlation).

with a diameter of ~2 mm after seven days of culture.

After seeding the MSCs in the constructs, the analogs were cultured statically for seven days to stimulate collagen synthesis and remodeling. During the culturing, a static uniaxial stretch along the long axis of the originally rectangular TE cap analogs, which corresponds to the circumferential direction, was applied. This loading/stretching condition was previously shown to induce fiber synthesis and remodeling parallel to the stretching direction induced by the Velcro constraints at the two ends of the TE cap (De Jonge et al., 2013; Wissing et al., 2022). The constructs were cultured in a base medium (αMEM (Gibco, Thermo Fisher Scientific, Breda, the Netherlands) containing 10 % heat-inactivated FBS (Sigma-Aldrich, St. Louis, USA), supplemented with 50 μg/mL gentamycin, 1.5 μg/mL fungizone, 50 μg/mL L-ascorbic acid 2- phosphate (Sigma-Aldrich, St. Louis, USA)) supplemented with 5 ng/ml TGF-β1. TGF-β1 was added to promote differentiation of the MSCs toward a smooth muscle cell (SMC)-like phenotype, creating a more physiologically relevant construct. MSCs we used instead of SMCs, because they are more readily accessible and proliferate rapidly (Afra and Matin, 2020; Gong and Niklason, 2008). On day seven, a 2 mm diameter soft inclusion was created by punching a hole in the center of each analog and filling it with fibrin (bovine fibrinogen (10 mg/ml) and bone thrombin (10 U/ml)). This collagen-poor inclusion with fibrin mechanically mimics the soft lipid core in human atherosclerotic plaques, whose stiffness was shown to be a few orders of magnitude lower than the fibrous plaque tissue (Duong et al., 2009; Wong et al., 2012). The analogs were then kept under the same static conditions for an additional fourteen days. Culturing was stopped on day 21 for collagen imaging and mechanical testing of the analogs. The samples (n = 43) underwent mechanical testing, a subset of these (n = 15) also were imaged.

2.2.3. Collagen architecture imaging and analysis

The subset of the analogs (n = 15, at least n = 4 for each group) was imaged using multiphoton microscopy. The analogs with HA clusters were incubated with an HA-targeting probe (IVISense Osteo 680 Fluorescent Probe, Osteosense, PerkinElmer), diluted 1:200 in culture medium for 24 h at 37 °C. After incubation, analogs were rinsed with Phosphate Buffered Saline (PBS) and were pinned to a silicone-filled (Sylgard 184, VWR, Germany) petri-dish using surgical needles to prevent movement during imaging. PBS was added to fully submerge the analogs. A laser scanning confocal microscope (TCS SP5, Leica, Germany) equipped with a Chameleon Ultra II multiphoton laser (Coherent, USA) was used to visualize the collagen architecture and HA clusters. First, a bright-field tile scan of the sample was made to localize HA clusters and soft inclusions. Subsequently, second harmonic generation (SHG) using two-photon microscopy (excitation at 880 nm) was employed to image collagen fibers in combination with confocal microscopy of the HA clusters (excitation at 680 nm). To minimize the scanning time to ~1 h per sample, only a portion of the analogs were imaged. This portion included at least 25 % of the analog, encompassing an entire calcification cluster along with both the luminal and abluminal sides of the cap analog. The selected tiles overlaid a part of the fibrous tissue of the analog, the HA clusters, and a part of the soft inclusion. Z-stacks (tile size 739 × 739 μm and pixel size 1.4 × 1.4 μm) were collected with a Z-step size of 9 μm up to a depth of approximately 200 μm from the surface that was facing downwards during culturing, as calcifications were predominantly visible on this side.

Maximum intensity projection (MIP) images were analyzed using CT-FIRE software (Bredfeldt et al., 2014), a MATLAB-based fiber orientation analysis tool, to identify individual collagen fibers and determine their orientations. Histograms of collagen fiber orientations in each tile were fitted with von Mises distributions. The predominant angle (θ) and the dispersion parameter (κ) of the collagen fibers per tile were extracted. θ is the mode of the von Mises distribution, and κ is a function of the height and width of the distribution as outlined in (Blaber et al., 2015). The dispersion parameter κ ranges from 0 to 1/3, where κ = 0 indicates perfect parallel alignment and κ = 1/3 indicates that the fibers exhibit a uniform distribution across all directions. For the interested reader, further methodological details on deriving these parameters from the von Mises fit can be found in Gasser et al. (2006).

2.2.4. Mechanical characterization: uniaxial tensile testing

All cap analogs (n = 43) were mechanically tested, including the imaged analogs, as previous studies showed MPM imaging had no significant effect on the mechanical properties of the analogs (Crielaard et al., 2025). First, high spatial resolution ultrasound imaging (Vevo 3100, FUJIFILM, Visual Sonics Inc., Canada) was performed to measure the cross-sectional areas of the analogs. A 2-D linear transducer with a 21 MHz central frequency (MX550) and a stepper motor were used to capture the cross-sectional area of the analogs at every 40 μm along the y-direction/circumferential direction (Fig. 1) of the analogs.

Subsequently, a speckle pattern for digital image correlation (DIC) analysis was applied to the surface of the analogs by using an airbrush filled with tissue dye (24113-2, Polysciences Inc., Ott Scientific). Then, the analogs were mounted to a custom-designed uniaxial tensile tester by placing the Velcro strips on each side of the analog in the clamps of the tensile tester. The clamps contained sandpaper (P400) and foam tape to prevent slippage of the analogs during the tests and were tightened to a torque of 10 cNm. The tensile tester was equipped with a 10 N load cell (LCMFD-10N, Omega Engineering, USA), and a linear actuator (EAC-M2E10AZAK, Oriental Motor, Japan).

Prior to testing, the analogs were visually inspected for any damage. Then, a pre-load of 0.05 N was applied to remove their slack. Subsequently, 10 cycles of preconditioning were performed, reaching up to 6 % strain, to ensure a repeatable mechanical response of the analogs (Humphrey and Delange, 2004; Walsh et al., 2014). Afterward, the analogs were stretched until failure at a speed of 200 %/min, to mimic the *in vivo* physiological pressures due to systole and diastole (Walsh et al., 2014). The specified strain and strain rate values were calculated using the clamp-to-clamp distance measured by the actuator right before pre-conditioning after the preload was applied. During testing, the analogs were fully submerged in PBS at 37 °C. A 12.2 Megapixel Camera (Imager CS2-12, LaVision, Germany) and a light source (KL 1500 LCD, Schott) were placed above the tensile tester to record videos of the analogs at 625 fps during testing. The captured camera images of the analog surfaces were used for DIC analysis and to determine the rupture initiation location later.

DIC analyses were conducted with StrainMaster software (DaVis 11, LaVision). The region of interest (ROI) was defined as the area of the analog, excluding ~1 mm from each clamp. Areas containing air bubbles in PBS were excluded from the analysis to prevent artifacts. Due to compaction in the central section during culturing, as previously observed (Jansen et al., 2023; Wissing et al., 2022), the analogs developed a dog bone-like shape, characterized by a reduction in width in the central region. This central area, referred to as the 'reduced section', is commonly employed for stress and strain assessment in uniaxial tensile testing (Macrae et al., 2016). In our analogs, the reduced section was defined as the region between two lines extending horizontally from the top and the bottom of the soft inclusion (Fig. 1).

The global tensile Green-Lagrange strain (ε_{yy}) was obtained by averaging the DIC-strain measurements within the reduced section of the analogs. The global tensile engineering stress (σ_{yy}) was calculated by dividing the measured tensile force by the initial average cross-sectional area in the reduced section. The tangent stiffness moduli of the analogs were calculated from the global stress-strain curves for every 0.025 strain increment up to the rupture initiation strain by performing linear regression on the data points of 0.0125 below and above these strain values.

Rupture initiation locations were identified by visual inspection of the camera images. The local tensile strains at the rupture initiation locations and the average tensile strains within the entire ROI of the analogs were calculated using DIC data.

2.3. Statistical analysis

Statistical analyses were conducted using MATLAB (Statistics and Machine Learning Toolbox, MathWorks, USA) and IBM SPSS Statistics (Version 29.0.1, IBM Corp, USA). The Shapiro-Wilk test was used to assess the normality of the data. For paired data comparisons within this study (e.g., strain values at the rupture initiation location versus average strain of the same analog), the Wilcoxon signed-rank test was used for non-normally distributed data, and the paired *t*-test for normally distributed data. For unpaired data (e.g., samples with luminal rupture versus samples with abluminal rupture), the Mann–Whitney *U* test was used for non-normally distributed data, and unpaired t-tests were performed for normally distributed data. If more than two groups were compared (e.g., Control, Luminal HA, and Abluminal HA), one-way ANOVA with Tukey's multiple comparison post hoc test was used for normally distributed data, and the Kruskal-Wallis test with a posthoc Dunn's comparison test for non-normally distributed data. Finally, if multiple measurements were performed per sample (e.g., dispersion measurements on multiple tiles), linear mixed models were employed to account for the dependency of the data points. A p-value <0.05 was considered statistically significant and represented as * $p < 0.05$, ** $p < 0.01$, *** $p < 0.001$.

3. Results

3.1. Localization of microcalcification clusters in real human carotid plaque caps

We analyzed the location of microcalcification clusters in human atherosclerotic carotid plaques, to ensure that the structural organization of the TE cap analogs accurately represented the *in vivo* variations observed In the 90 histological human carotid cross-sections from seven endarterectomy donors, 14 cross-sections contained microcalcifications within the plaque cap. The microcalcifications were present in clusters. In total, 23 microcalcification clusters were identified which had shapes elongated in the circumferential direction, as previously reported (Jansen et al., 2023). These clusters had a variable composition, with small (<5 μm) and bigger (>5 μm and <50 μm) microcalcifications being present within the clusters in varying densities. In 35 % ($n = 8$, Fig. 2A) of the sections, the clusters were on the luminal side only, while 43 % ($n = 10$, Fig. 2A) of the cross-sections showed clusters only on the lipid core side. The remainder of the cross-sections (22 %, $n = 5$) included clusters with no clear predisposition towards one of the two sides.

HA clusters in the TE analogs were created at either the luminal or abluminal (lipid-core) side to mimic the two distinct groups observed in the real human plaques. TE analogs were created such that the HA clusters would mimic the microcalcification clusters in real plaques (Fig. 2B), including features such as the clusters located along the circumferential direction, as observed in human carotid plaque caps. Moreover, the particle size and density of the HA clusters were ensured to be similar to those in human plaques, as previously characterized (Jansen et al., 2023)

3.2. TE analog geometry and microstructural architecture

The analogs had a length of ~10 mm (clamp-to-clamp length) and a total width of ~7 mm in the reduced section. The SIs had a length of ~3 mm and a width of ~2 mm. The reduced section demonstrated a thickness of ~0.3 mm.

Collagen fibers in the analogs (Control: $n = 4$, Luminal HA: $n = 6$, Abluminal HA: $n = 5$) were predominantly oriented close to the vertical y-direction ($\theta = 90°$) (mean $\theta \pm$ SD: control group = $100° \pm 7°$, luminal HA group = $94° \pm 8°$, abluminal HA group = $97° \pm 8°$). Fig. 3A shows the multiphoton microscopy images (left) and the corresponding fiber organization analysis results (right) for an analog from each group. The fibers at the luminal and abluminal regions were observed to be parallel to the edge contours for all analogs (Fig. 3A). No significant differences in the average predominant fiber angle and dispersion (κ) were found between the three groups (control and luminal HA group = 0.15 ± 0.04, abluminal HA group = 0.10 ± 0.03).

However, regional differences in dispersion were observed within and between the groups. The fibers in the luminal region in all three groups showed significantly less dispersion than the abluminal region (Fig. 3B, mean $\kappa \pm$ SD: control group = 0.09 ± 0.05 vs 0.19 ± 0.04 ($p < 0.05$), luminal HA group = 0.11 ± 0.03 vs 0.18 ± 0.05 ($p < 0.01$), and abluminal HA group = 0.06 ± 0.01 vs 0.17 ± 0.04 ($p < 0.001$)). Moreover, when luminal regions (Fig. 3A, the three columns of tiles at the luminal side) were compared, the abluminal HA group showed significantly lower dispersion than the luminal HA group ($p < 0.01$, 0.06 vs. 0.11) (Fig. 3B).

3.3. Global mechanical properties of the TE analogs

Of the 43 analogs tested mechanically, three were excluded from subsequent analyses due to a clamp rupture, poor speckle pattern quality, or the presence of excessive air bubbles in the PBS, which affected the DIC analysis. The average transversal cross-sectional area in the reduced section of the analyzed analogs ($n = 40$) was 1.61 ± 0.36 mm^2.

The three groups showed similar stress-strain responses (Fig. 4A) and stiffness (Fig. 4B). The median [IQR] stiffness value at 0.05 strain (Fig. 4B) was 4.1 MPa [3.4:5.0] for the control group, 3.1 MPa [1.1:4.1] for the abluminal HA group, and 3.5 MPa [3.0:4.5] for the luminal HA group. Tensile failure stress in the abluminal group was significantly lower ($p < 0.05$) than the one in the control group (Fig. 4C and 0.23 MPa [0.19:0.45] vs. 0.43 MPa [0.38:0.47]). The tensile failure stress was 0.29 MPa [0.22:0.38] for the luminal HA group, which was also lower than the control group, although there was no statistical significance. Similarly, the groups with HA clusters had lower tensile failure strain than the control group (Fig. 4D). The difference was statistically significant for both the abluminal HA ($p < 0.05$) and luminal HA ($p < 0.01$) groups compared to the control group (0.06 [0.05:0.09] and 0.07 [0.05:0.08], respectively, vs. 0.10 [0.08:0.11]). However, it is important to note the considerable variability observed in the sample-level data, especially in the samples with microcalcifications, which may complicate the generalizability of these correlations based on group average.

3.4. Rupture initiation location

In the majority of the control group analogs, abluminal rupture was observed, while in a small number, rupture initiated in a region not clearly defined as either luminal or abluminal, which we termed the mid-tissue (85 % vs. 15 %, Fig. 5A). All abluminal HA group analogs demonstrated the rupture initiation at the abluminal side. In the luminal HA group, approximately half (47 %) of the samples had the tissue rupture initiating at the luminal side, while the other half at the abluminal side. Further investigation of the luminal HA group (Fig. 5B) demonstrated that the analogs with a rupture initiation at the luminal side had the HA cluster closer to the lumen (9 ± 25 vs. 289 ± 186 μm, $p < 0.01$).

3.5. Local mechanics at rupture initiation location

In Fig. 6A, the DIC-derived local tensile strain (ε_{yy}) measurements of a representative analog from each group are shown right before the rupture initiation in the fibrous tissue. No significant correlation was found between local collagen fiber orientation and dispersion with the average and maximum local strain within each imaged tile. However, rupture initiation was consistently found in high-strain regions, and in 86 % of the analogs even at the highest strain location in the sample. The median tensile strain at the rupture locations was 0.15 [0.11:0.21] at the

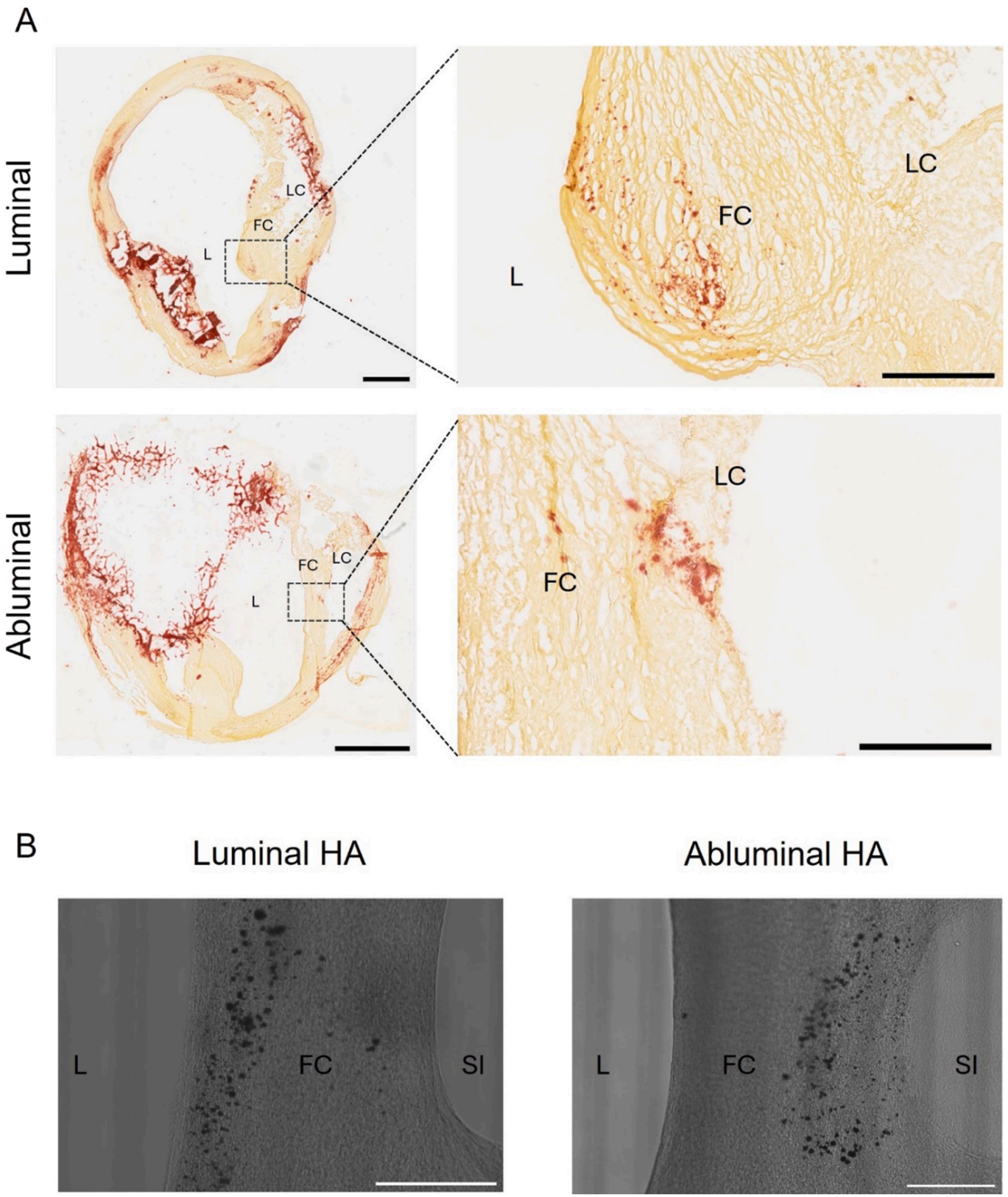

Fig. 2. Location of A) microcalcification clusters in human carotid atherosclerotic plaque caps (Alizarin Red staining, microcalcifications in red) and B) Brightfield images of HA clusters in tissue-engineered fibrous cap analogs. (Scale bars: A) 2 mm and zoom 500 μm, B) 1 mm) (L = lumen, FC = fibrous cap, LC = lipid core, SI = Soft Inclusion). (For interpretation of the references to color in this figure legend, the reader is referred to the Web version of this article.)

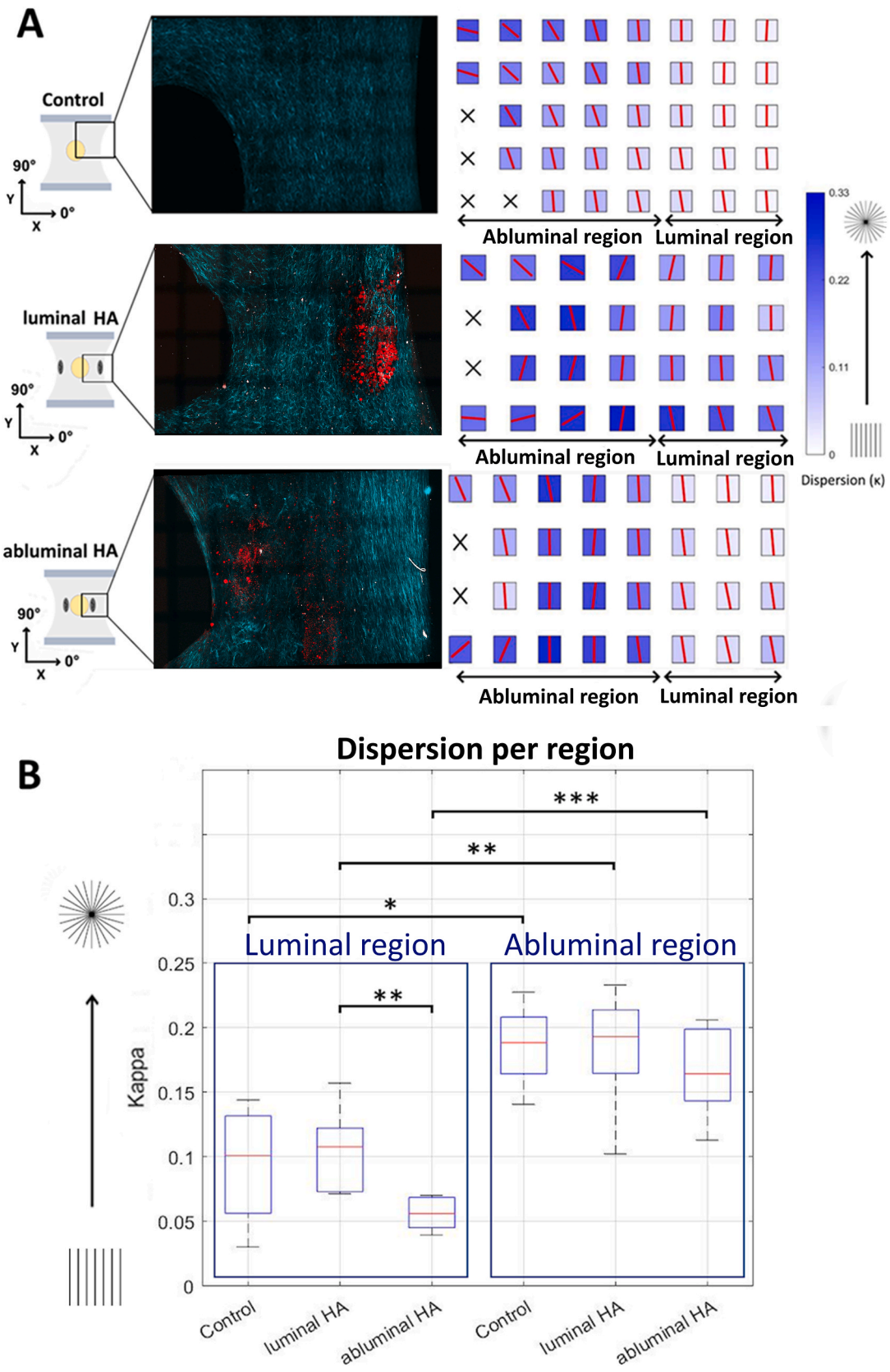

Fig. 3. A) Left: Multiphoton microscopy images of a TE analog from each of the three groups, collagen in green and HA particles in red (stained with Osteosense), and Right: local predominant fiber orientation (red line) and dispersion, κ, (background color) with abluminal and luminal regions indicated. B) Average fiber dispersion in the luminal and abluminal regions per group (Control, Luminal HA, and Abluminal HA). (*$p < 0.05$, **$p < 0.01$, ***$p < 0.001$; Boxplots show median [IQR]). (For interpretation of the references to color in this figure legend, the reader is referred to the Web version of this article.)

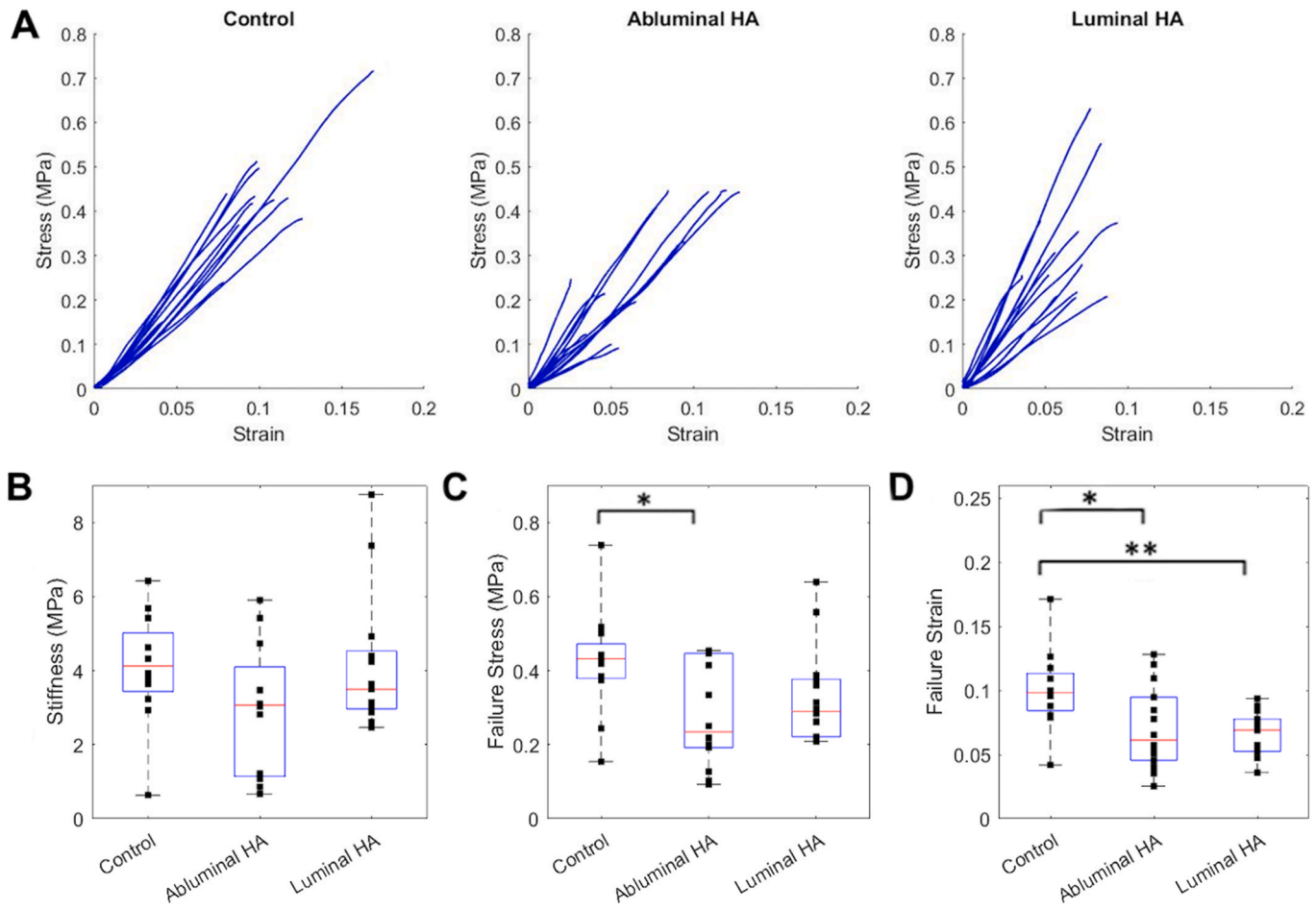

Fig. 4. Global mechanical properties of the TE analogs. (*p < 0.05, **p < 0.01; Boxplots show median [IQR])) A) Tensile stress-strain response of the three groups B) Stiffness at 0.05 strain, C) Failure stress, and D) Failure strain.

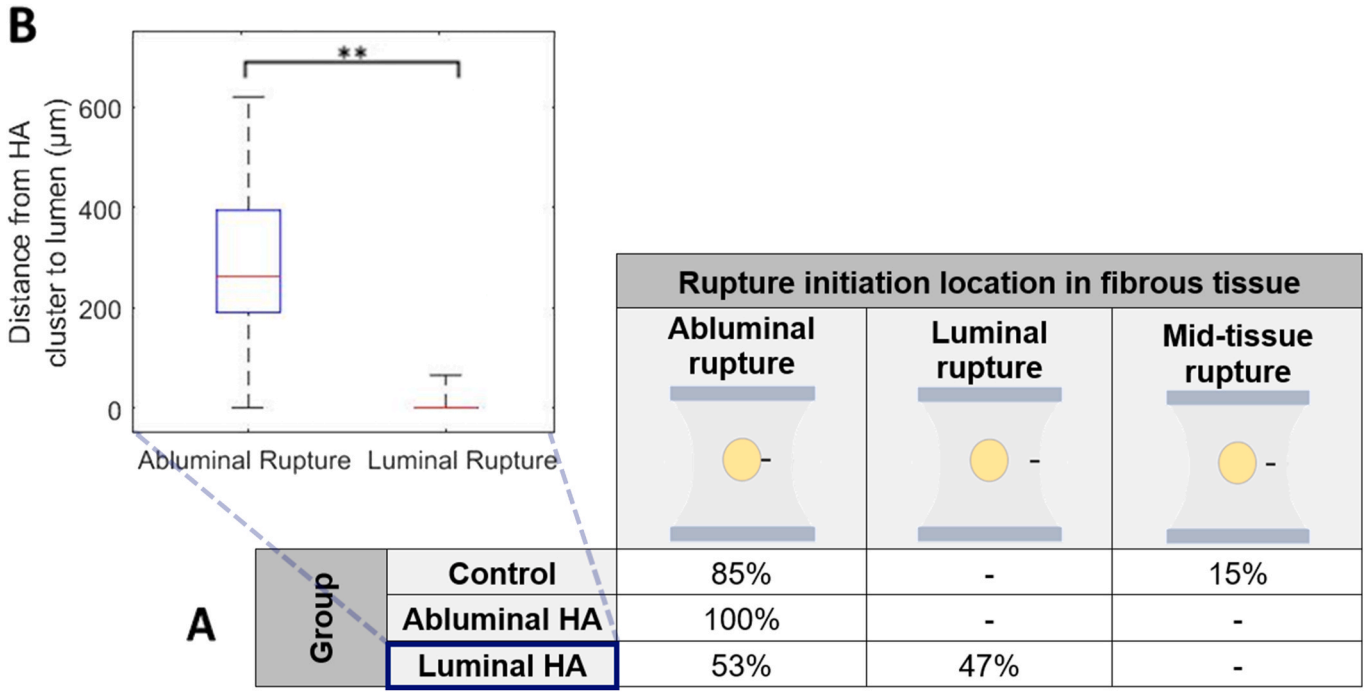

Fig. 5. A) Rupture initiation location in the fibrous tissue of our analogs B) Quantification of the distance (µm) of the HA clusters to the lumen in the luminal HA group, luminal rupture analogs vs. abluminal rupture analogs (**p < 0.01; Boxplots show median [IQR]).

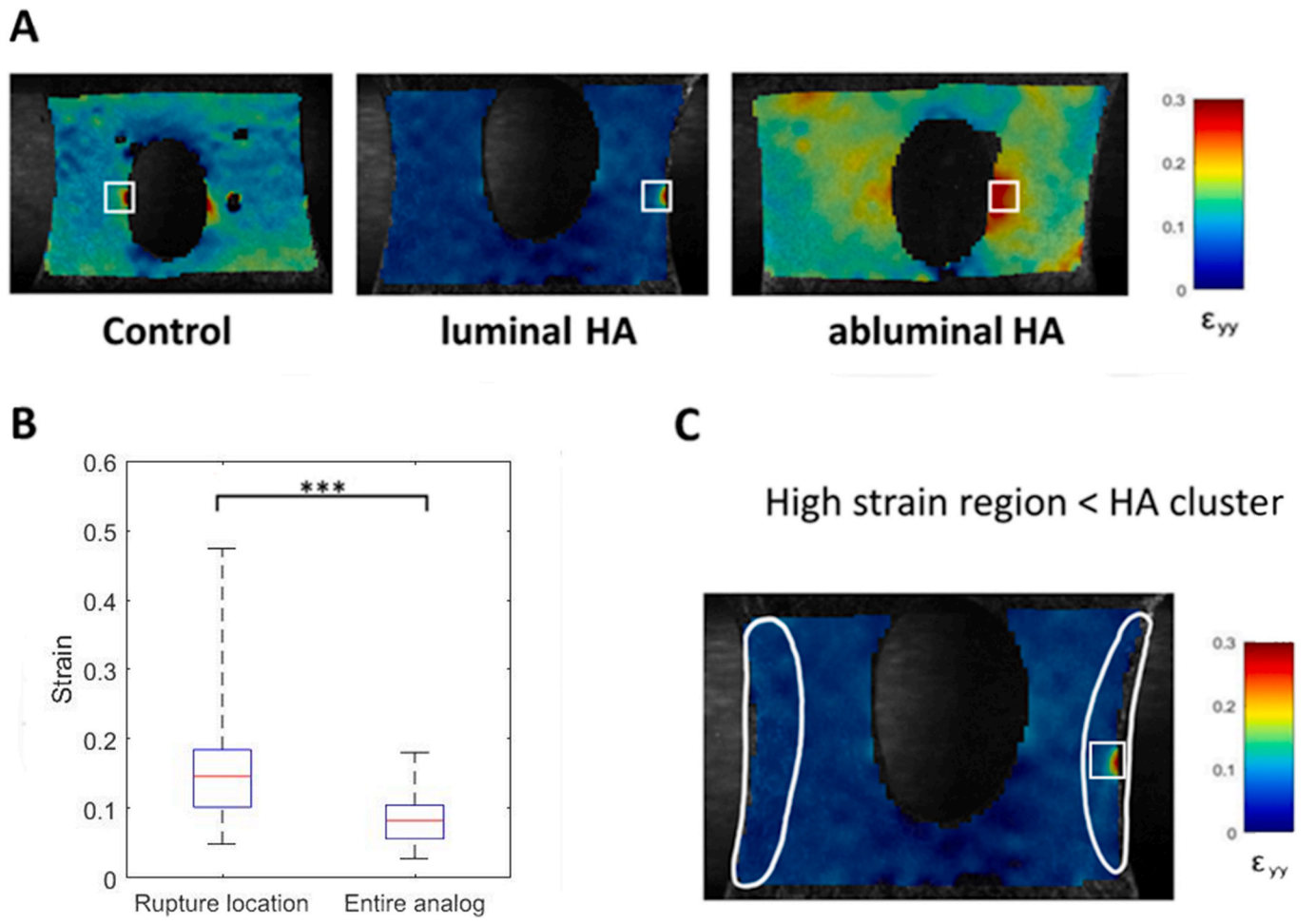

Fig. 6. A) DIC-derived tensile strain (ε_{yy}) distribution right before rupture initiation in representative analogs. The white box marks the rupture initiation location. B) Average tensile strain (ε_{yy}) at the rupture initiation site and in the entire analog. (***$p < 0.001$; Boxplots show median [IQR]) C) Overlay of the HA cluster location (white ellipsoidal region) and rupture initiation location (white box) on the DIC-derived tensile strain ($\varepsilon_{yy.}$), highlighting the small size of the high-strain region relative to the entire HA cluster.

rupture initiation site, whereas the median strain within the analogs was 0.08 [0.06:0.10] ($p < 0.001$, Fig. 6B). No significant differences were found in the local tensile failure strain at the rupture initiation site between the groups (Median [IQR] = control group: 0.16 [0.11:0.17], luminal HA group: 0.11 [0.10:0.16], and abluminal HA group: 0.15 [0.14:0.23]). The high-strain spots were often more than 20 times smaller than the size of the entire calcification cluster (Fig. 6C).

4. Discussion

The examination of human carotid plaque caps revealed a localized presence of microcalcifications in clusters (Jansen et al., 2023). These clusters demonstrated shapes elongated in the circumferential arterial direction. This study performs the first analysis in carotid arteries concerning the localization of microcalcification clusters from the lumen to the lipid core. Approximately 80 % of these clusters were located either at the luminal side or at the abluminal side (the lipid core side). The clusters located at the luminal side might be formed due to osteogenic trans-differentiation of vascular smooth muscle present in the cap (Otsuka and et al., 2014), while clusters at the lipid core side might initiate on cellular debris present in the necrotic core (Neels et al., 2023).

The cultured TE cap analogs mimicked the collagen fiber organization of real human caps (Crielaard et al., 2025). The collagen fibers were mainly oriented around the y-direction, which corresponds to the predominant circumferential direction in human plaques (Akyildiz et al., 2017; Johnston et al., 2021). Moreover, the luminal regions demonstrated lower dispersion, implying a more parallel alignment. Since global failure stress and strain are determined by the timepoint of local rupture, regional structural differences can significantly influence these global outcomes. Similar collagen organization was reported before for human plaque caps (Douglas et al., 2017). The highest dispersion within our samples was observed in the abluminal region. This might be due to increased stretching in directions other than the loading direction during culture. Multidirectional stretching was previously shown to decrease collagen alignment in the main loading direction (Foolen et al., 2012). We anticipate that this arises from geometric factors such as the positioning of the soft inclusion in our TE samples. Additionally, differences in loading may occur due to local differences in stress and strain due to compaction during culture.

Next, the effect of HA particles on the local fiber organization was assessed. Considering the abluminal regions of the samples, no significant differences were observed between the experimental groups. This is likely due to the fact that the dispersion was already high in this region, causing no effect of the addition of microcalcifications within this region. For the luminal region, a significantly higher dispersion was observed in the luminal HA group compared to the same region of the abluminal HA group. This may indicate that the presence of HA clusters in this luminal region disturbed the organized parallel alignment of the collagen fibers. This disturbance of aligned fibers due to

microcalcifications has been observed before in previous research and might be a possible reason for the altered mechanical properties (Jansen et al., 2023). This effect however, seems to be rather small, because no significant differences in dispersion were observed between the luminal regions in the HA groups and the control group.

Uniaxial tensile tests revealed that all samples demonstrated stress-strain responses comparable to human plaques, measured *ex vivo* (Johnston et al., 2021; Torun et al., 2023). The observed stiffness values fall within the range reported for human fibrous caps (0.1–5 MPa (Akyildiz et al., 2014). The analogs also showed global failure strain and stress values that were within the range reported for human fibrous caps and plaque tissue (0.04–0.23 and 0.1–2.0 MPa, respectively) (Johnston et al., 2021; Torun et al., 2023).

When comparing the control group with the two HA groups, no statistically significant differences were found in global stiffness, likely because the HA particles occupy only a small fraction of the entire sample. However, the failure tensile strain and stress were lower for the HA groups than the control group, indicating a critical impact of the microcalcifications' presence on rupture risk, regardless of their location. The fact that no differences were observed in stiffness in the current study, but failure stress and strain were lowered, could suggest that the mechanical effect of microcalcifications is very localized. Based on these results, one can hypothesize that local stress and strain concentrations in the microcalcification cluster regions lead to micro-damage and consequent tissue rupture, which provides the long-awaited experimental evidence for computational models (Corti and et al., 2022; Maldonado et al., 2013). However, a considerable variability in the sample-level data was also observed. Notably, the variability was most pronounced in samples containing microcalcifications, suggesting that factors beyond microcalcification location, such as calcification density and its secondary effects on local collagen dispersion and fiber orientation, may also influence mechanical behavior.

As observed previously, the analogs in the control group ruptured mainly at the abluminal edge, with some ruptures initiating in the mid-tissue. Interestingly, all samples in the abluminal HA group ruptured at the abluminal edge, which might indicate the potential influence of HA cluster presence on rupture location. This was further evidenced when the luminal HA group was analyzed. In this group approximately half of the samples ruptured at the luminal side, while the other half ruptured at the abluminal side. This is particularly intriguing because luminal ruptures were not observed in previous studies utilizing TE caps (Crielaard et al., 2025; Wissing et al., 2022). Further investigation of the luminal HA group demonstrated that the analogs that ruptured at the luminal side had HA clusters statistically significantly closer to the lumen. These findings indicate that the rupture initiation location shifts toward the site of microcalcifications.

No significant correlation was found between local collagen fiber orientation and dispersion with the local strain within each imaged tile. While these local structural features likely contribute to local strain patterns, the substantial nonuniformity in other mechanical and structural factors, such as regional variations in load distribution, local geometry, and interactions with neighboring regions, complicates the ability to isolate and quantify their individual effects.

Our DIC analysis revealed that rupture initiation consistently occurred in high-strain regions in all analogs, regardless of the presence of HA clusters, with strain values approximately twice as high as the overall strain in the analogs. Rupture initiation was found at the highest strain region in 86 % of the samples, indicating a strong association between high local strain values and cap rupture. Our findings highlight the critical importance of acquiring local strain data of plaque tissue rather than relying on gross, averaged values, which assume tissue homogeneity, as is commonly done in studies on plaque mechanics. Moreover, these findings suggest the potential use of local strain measurements as a new marker for plaque rupture risk prediction. Previously, cap stresses, which require computational modeling, were proposed for improved rupture risk prediction (Milzi et al., 2021). However, local strain as a marker has the advantage over stress as it could be obtained *in vivo* more easily using clinical imaging techniques like ultrasound (Schaar et al., 2003). This technique is especially easy to use for carotid arteries, since it is a non-invasive technique for these plaques (Hansen et al., 2016). Cap strain imaging could allow for long-term monitoring of plaque characteristics, disease progression and the effectiveness of treatments (Hansen et al., 2016). Since traditional evaluation often has low predictive values for clinical events (SCOT-HEART Investigators, 2018), new markers for plaque rupture, such as these local strain measurements, could help to better identify patients at risk.

Furthermore, for samples containing HA clusters, we observed that the regions of high strain were localized within the clusters, although these high-strain regions were smaller than the clusters themselves. This could be due to local variations in HA particle density, which may lead to areas of relatively higher and lower strain within the clusters, as density and local distance between microcalcifications have been shown to influence cap mechanics (Corti et al., 2023; Wenk, 2011).

There are some limitations associated with this study. Human plaques are under a multiaxial loading state *in vivo*, which is more complex than the uniaxial tensile loading applied to the cap analogs in the current study. However, the dominant *in vivo* loading is circumferential tensile loading. Hence, the uniaxial tensile loading applied to the cap analogs in the current study is the most relevant one. Another limitation is that collagen fiber orientation was not assessed in the axial direction, but only in the radial-circumferential plane. Although the TE cap analogs were stretched in the circumferential direction during culturing and hence, fibers were expected to align predominantly in this direction. While MPM imaging can capture in-plane fiber information in the imaging plane in great detail and spatial resolution, the out-of-plane information is poorly acquired by MPM. Especially given the current z-step size, which is relatively large due to the need to accelerate imaging in order to complete sufficient data collection before mechanical testing. Therefore, our analyses were limited to circumferential-radial plane information of the fibers. Moreover, in the current study, we assumed purely elastic mechanical behavior of the TE cap analogs. Similarly, real atherosclerotic plaque tissue is commonly assumed to be linear elastic (Loree et al., 1994); however, some recent studies suggested viscoelastic features of the tissue (Leng et al., 2018). Plaque regions with higher necrosis and lipid content have been shown to demonstrate more viscous behavior, making these areas supposedly more prone to greater deformation and damage (Chang et al., 2023; 2024; Zhou et al., 2022). Future research could expand our current study by exploring the viscoelastic behavior of TE caps, changes in its composition, and the potential implications for plaque stability. Another limitation is the relative simplicity of the tissue-engineered cap analogs' structure compared to human plaque caps. The current model includes a collagenous matrix and microcalcifications, which are two of the main determinants hypothesized to play a role in plaque rupture (Jansen et al., 2024). However, more disease characteristics such as lipids within the soft inclusion and inflammatory cells could be introduced to more accurately replicate the complex characteristics of human plaques. Additionally, the collagenous matrix is known to be a heterogeneous structure with differences in density, type, and crosslinking (Jansen et al., 2024). The matrix in the TE analogs could be altered by introducing compounds like ribose, copper, or beta-aminopropionitrile during culture. These modifications could promote advanced glycation end-product (AGE)-related crosslinking and modulate lysyl oxidase (LOX)-mediated crosslinking (Beekman et al., 1997; Dahl et al., 2005; Gouldin et al., 2020; Melike et al., 2018). To assess more heterogeneous characteristics of microcalcifications, our TE cap model can be used to investigate additional structural parameters. First, future research could quantify local density of HA particles within our TE cap analogs to assess its impact on local strain patterns. Second, microcalcifications are known to be distributed from the mid-cap to the shoulder region non-uniformly (Maldonado and et al., 2012), with numerical studies indicating that this distribution

influences local stress (Wenk, 2011; Wenk et al., 2010). The TE model could be utilized to create HA clusters positioned in either the mid-cap or shoulder region. Moreover, future research should experimentally assess how HA particle shape affects plaque stability. In our study, we used round-shaped particles that resemble a common type of micro-calcification (Supplementary Fig. 1). Future work could introduce different HA particle shapes into tissue-engineered caps and combine high-resolution imaging with mechanical testing to better understand their impact on fibrous cap integrity. Lastly, our current study examines the impact of an HA cluster, whereas human caps may contain multiple clusters (Jansen et al., 2023). Future experimental studies could investigate the mechanical effects of multiple HA clusters to better replicate *in vivo* conditions (Jansen et al., 2023). Our TE analogs thus offer great flexibility and control over various structural parameters, making them a great platform to examine the impact of these parameters on mechanical properties and rupture behavior.

In this study, HA clusters were introduced into the TE caps to simulate microcalcifications. Although this technique allows for precise control over variables like amount and location, developing a TE cap model that generates microcalcifications through cellular processes would better replicate *in vivo* conditions. Several theories have been proposed for the formation of microcalcifications. For example, the osteogenic differentiation of plaque-resident vascular smooth muscle cells (VSMCs) (Durham et al., 2018). Other mechanisms include calcifying extracellular vesicles (New and Aikawa, 2013), apoptosis of plaque-resident cells (Clarke et al., 2008), and the loss of calcification inhibitors. Our TE model can be adapted to investigate these pathways. For example, extracellular vesicles can be harvested and incorporated into the TE caps, following the methodology described by Hutcheson (2016). Additionally, apoptosis may be triggered within the model by activating apoptosis receptors or applying chemical agents (Proudfoot et al., 2001).

5. Conclusion

In this study, we investigated how the presence and location of microcalcification clusters influence the global and local cap mechanics, and rupture behavior of atherosclerotic fibrous cap analogs. Using tissue-engineered fibrous cap analogs with HA clusters, we replicated the microcalcification distribution observed in human carotid plaques, as observed in our histological analysis.

Our results demonstrated the effect of the HA clusters on the collagen fiber organization, causing more dispersion of the fibers locally, particularly if present on the luminal side. The presence of the HA clusters reduced both the failure tensile stress and strain, indicating that the fibrous cap becomes more prone to rupture. Moreover, our results indicate that HA clusters relocate the location of the rupture. Additionally, high local strains were measured at the rupture sites, with these spots being highly localized—often much smaller than the size of the entire HA cluster. This finding may suggest the potential benefit of using in-vivo local strain measurement as an additional marker for assessing plaque rupture risk.

CRediT authorship contribution statement

Hanneke Crielaard: Writing – review & editing, Writing – original draft, Project administration, Methodology, Investigation, Formal analysis, Data curation, Conceptualization. **Imke Jansen:** Writing – review & editing, Writing – original draft, Project administration, Methodology, Investigation, Formal analysis, Data curation, Conceptualization. **Kim van der Heiden:** Writing – review & editing, Supervision, Conceptualization. **Gert-Jan Kremers:** Writing – review & editing, Methodology. **Frank J.H. Gijsen:** Writing – review & editing, Supervision, Conceptualization. **Eric Farrell:** Writing – review & editing, Supervision, Methodology. **Ali C. Akyildiz:** Writing – review & editing, Supervision, Conceptualization.

Funding statement

This work was supported by an NWO-Vidi grant [18360]; and the European Research Council (ERC) under Horizon Europe 2020 research and innovation program [101042724 — MicroMechAthero].

Declaration of competing interest

The authors declare that they have no known competing financial interests or personal relationships that could have appeared to influence the work reported in this paper.

Appendix A. Supplementary data

Supplementary data to this article can be found online at https://doi.org/10.1016/j.jmbbm.2025.107139.

Data availability

Data will be made available on request.

References

Afra, S., Matin, M.M., 2020. Potential of mesenchymal stem cells for bioengineered blood vessels in comparison with other eligible cell sources. Cell Tissue Res. 380, 1–13. https://doi.org/10.1007/s00441-019-03161-0.

Aikawa, E., et al., 2007. Osteogenesis associates with inflammation in early-stage atherosclerosis evaluated by molecular imaging in vivo. Circulation 116, 2841–2850.

Akyildiz, A.C., Chai, C.K., Oomens, C.W.J., van der Lugt, A., Baaijens, F.P.T., Strijkers, G. J., Gijsen, F.J.H., 2017. 3D Fiber orientation in atherosclerotic carotid plaques. J. Struct. Biol. 200, 28–35. https://doi.org/10.1016/j.jsb.2017.08.003.

Akyildiz, A.C., Speelman, L., Gijsen, F.J.H., 2014. Mechanical properties of human atherosclerotic intima tissue. J. Biomech. 47, 773–783. https://doi.org/10.1016/j.jbiomech.2014.01.019.

Beekman, B., Verzijl, N., Bank, R., Mark, K., Tekoppele, J., 1997. Synthesis of collagen by bovine chondrocytes cultured in alginate; posttranslational modifications and cell–matrix interaction. Exp. Cell Res. 237, 135–141. https://doi.org/10.1006/excr.1997.3771.

Blaber, J., Adair, B., Antoniou, A., 2015. Ncorr: Open-Source 2D digital image correlation Matlab software. Exp. Mech. 55, 1105–1122. https://doi.org/10.1007/s11340-015-0009-1.

Bluestein, D., et al., 2008. Influence of microcalcifications on vulnerable plaque mechanics using FSI modeling. J. Biomech. 41, 1111–1118.

Bredfeldt, J.S., Liu, Y., Pehlke, C.A., Conklin, M.W., Szulczewski, J.M., Inman, D.R., Keely, P.J., Nowak, R.D., Mackie, T.R., Eliceiri, K.W., 2014. Computational segmentation of collagen fibers from second-harmonic generation images of breast cancer. J. Biomed. Opt. 19, 16007. https://doi.org/10.1117/1.JBO.19.1.016007.

Chang, Z., Zhang, J., Liu, Y., Gao, H., Xu, G.-K., 2023. New mechanical markers for tracking the progression of myocardial infarction. Nano Lett. 23, 7350–7357. https://doi.org/10.1021/acs.nanolett.3c01712.

Cilla, M., Monterde, D., Pena, E., Martinez, M.A., 2013. Does microcalcification increase the risk of rupture? Proc. Inst. Mech. Eng., Part H 227, 588–599.

Clarke, M.C.H., Littlewood, T.D., Figg, N., Maguire, J.J., Davenport, A.P., Goddard, M., Bennett, M.R., 2008. Chronic apoptosis of vascular smooth muscle cells accelerates atherosclerosis and promotes calcification and medial degeneration. Circ. Res. 102, 1529–1538. https://doi.org/10.1161/CIRCRESAHA.108.175976.

Corti, A., et al., 2022. The effect of plaque morphology, material composition and microcalcifications on the risk of cap rupture: a structural analysis of vulnerable atherosclerotic plaques. Front. Cardiovasc. Med. 9, 2875.

Corti, A., Khalil, D., De Paolis, A., Cardoso, L., 2023. Size and proximity of micro-scale hard-inclusions increase the risk of rupture in fibroatheroma-like laboratory models. J. Mech. Behav. Biomed. Mater. 141, 105749.

Crielaard, H., Wissing, T.B., Guvenir Torun, S., Kremers, G.-J., de Miguel, P., Hengst, R. M., Gijsen, F.J.H., Akyildiz, A.C., van der Heiden, K., 2025. Local characterization of collagen architecture and mechanical properties of tissue engineered atherosclerotic plaque cap analogs. Acta Biomater. https://doi.org/10.1016/j.actbio.2025.01.035.

Cullen, P., Baetta, R., Bellosta, S., Bernini, F., Chinetti, G., Cignarella, A., von Eckardstein, A., Exley, A., Goddard, M., Hofker, M., Hurt-Camejo, E., Kanters, E., Kovanen, P., Lorkowski, S., McPheat, W., Pentikäinen, M., Rauterberg, J., Ritchie, A., Staels, B., Weitkamp, B., de Winther, M., 2003. Rupture of the atherosclerotic plaque. Arterioscler. Thromb. Vasc. Biol. 23, 535–542. https://doi.org/10.1161/01.ATV.0000060200.73623.F8.

Dahl, S.L.M., Rucker, R.B., Niklason, L.E., 2005. Effects of copper and cross-linking on the extracellular matrix of tissue-engineered arteries. Cell Transplant. 14, 367–374. https://doi.org/10.3727/000000005783982936.

De Jonge, N., Kanters, F.M.W., Baaijens, F.P.T., Bouten, C.V.C., 2013. Strain-induced collagen organization at the micro-level in fibrin-based engineered tissue constructs. Ann. Biomed. Eng. 41, 763–774.

Douglas, G.R., Brown, A.J., Gillard, J.H., Bennett, M.R., Sutcliffe, M.P.F., Teng, Z., 2017. Impact of fiber structure on the material stability and rupture mechanisms of coronary atherosclerotic plaques. Ann. Biomed. Eng. 45, 1462–1474. https://doi.org/10.1007/s10439-017-1827-3.

Duong, H., Wu, B., Tawil, B., 2009. Modulation of 3D fibrin matrix stiffness by intrinsic fibrinogen–thrombin compositions and by extrinsic cellular activity. Tissue Eng Part A 15, 1865–1876. https://doi.org/10.1089/ten.tea.2008.0319.

Durham, A.L., Speer, M.Y., Scatena, M., Giachelli, C.M., Shanahan, C.M., 2018. Role of smooth muscle cells in vascular calcification: implications in atherosclerosis and arterial stiffness. Cardiovasc. Res. 114, 590–600. https://doi.org/10.1093/cvr/cvy010.

Foolen, J., Deshpande, V.S., Kanters, F.M.W., Baaijens, F.P.T., 2012. The influence of matrix integrity on stress-fiber remodeling in 3D. Biomaterials 33, 7508–7518. https://doi.org/10.1016/j.biomaterials.2012.06.103.

Gasser, T.C., Ogden, R.W., Holzapfel, G.A., 2006. Hyperelastic modelling of arterial layers with distributed collagen fibre orientations. J. R. Soc. Interface 3, 15–35. https://doi.org/10.1098/rsif.2005.0073.

Gijsen, F.J.H., Vis, B., Barrett, H.E., Zadpoor, A.A., Verhagen, H.J., Bos, D., van der Steen, A.F.W., Akyildiz, A.C., 2021. Morphometric and mechanical analyses of calcifications and fibrous plaque tissue in carotid arteries for plaque rupture risk assessment. IEEE Trans. Biomed. Eng. 68, 1429–1438. https://doi.org/10.1109/TBME.2020.3038038.

Gong, Z., Niklason, L.E., 2008. Small-diameter human vessel wall engineered from bone marrow-derived mesenchymal stem cells (hMSCs). FASEB J. 22, 1635–1648. https://doi.org/10.1096/fj.07-087924.

Gouldin, A.G., Brown, M.E., Puetzer, J.L., 2020. An inducible model for unraveling the effects of advanced glycation end-product accumulation in aging connective tissues. https://doi.org/10.1101/2020.09.04.283473.

Hansen, H.H.G., de Borst, G.J., Bots, M.L., Moll, F.L., Pasterkamp, G., de Korte, C.L., 2016. Validation of noninvasive in vivo compound ultrasound strain imaging using histologic plaque vulnerability features. Stroke 47, 2770–2775. https://doi.org/10.1161/STROKEAHA.116.014139.

Heiden, K. Van der, Hoogendoorn, A., Daemen, M.J., Gijsen, F.J.H., 2016. Animal models for plaque rupture: a biomechanical assessment. Thromb. Haemost. 115, 501–508. https://doi.org/10.1160/th15-07-0614.

Humphrey, J.D., Delange, S.L., 2004. An Introduction to Biomechanics. Springer, New York, New York, NY. https://doi.org/10.1007/978-1-4899-0325-9.

Hutcheson, J.D., et al., 2016. Genesis and growth of extracellular-vesicle-derived microcalcification in atherosclerotic plaques. Nat. Mater. 15, 335–343.

Jang, I.-K., Tearney, G.J., MacNeill, B., Takano, M., Moselewski, F., Iftima, N., Shishkov, M., Houser, S., Aretz, H.T., Halpern, E.F., Bouma, B.E., 2005. In vivo characterization of coronary atherosclerotic plaque by use of optical coherence tomography. Circulation 111, 1551–1555. https://doi.org/10.1161/01.CIR.0000159354.43778.69.

Jansen, I., Cahalane, R., Hengst, R., Akyildiz, A., Farrell, E., Gijsen, F., Aikawa, E., van der Heiden, K., Wissing, T., 2024. The interplay of collagen, macrophages, and microcalcification in atherosclerotic plaque cap rupture mechanics. Basic Res. Cardiol. 119, 193–213. https://doi.org/10.1007/s00395-024-01033-5.

Jansen, I., Crielaard, H., Wissing, T., Bouten, C., Gijsen, F., Akyildiz, A.C., Farrell, E., van der Heiden, K., 2023. A tissue-engineered model of the atherosclerotic plaque cap: toward understanding the role of microcalcifications in plaque rupture. APL Bioeng. 7. https://doi.org/10.1063/5.0168087.

Johnston, R.D., Gaul, R.T., Lally, C., 2021. An investigation into the critical role of fibre orientation in the ultimate tensile strength and stiffness of human carotid plaque caps. Acta Biomater. 124, 291–300. https://doi.org/10.1016/j.actbio.2021.02.008.

Kelly-Arnold, A., et al., 2013. Revised microcalcification hypothesis for fibrous cap rupture in human coronary arteries. Proc. Natl. Acad. Sci. U. S. A. 110, 10741–10746.

Kwak, B.R., Bäck, M., Bochaton-Piallat, M.-L., Caligiuri, G., Daemen, M.J.A.P., Davies, P. F., Hoefer, I.E., Holvoet, P., Jo, H., Krams, R., Lehoux, S., Monaco, C., Steffens, S., Virmani, R., Weber, C., Wentzel, J.J., Evans, P.C., 2014. Biomechanical factors in atherosclerosis: mechanisms and clinical implications. Eur. Heart J. 35 (3013–20). https://doi.org/10.1093/eurheartj/ehu353, 3020a-3020d.

Leng, X., Zhou, B., Deng, X., Davis, L., Sutton, M.A., Shazly, T., Lessner, S.M., 2018. Determination of viscoelastic properties of human carotid atherosclerotic plaque by inverse boundary value analysis. IOP Conf. Ser. Mater. Sci. Eng. 381, 012171. https://doi.org/10.1088/1757-899X/381/1/012171.

Loree, H.M., Grodzinsky, A.J., Park, S.Y., Gibson$, L.J., Lee, R.T., 1994. Static circumferential tangetial modulus of human atherosclerotic tissue. J. Biomech.

Macrae, R.A., Miller, K., Doyle, B.J., 2016. Methods in mechanical testing of arterial tissue: a review. Strain 52, 380–399. https://doi.org/10.1111/str.12183.

Maldonado, N., et al., 2012. A mechanistic analysis of the role of microcalcifications in atherosclerotic plaque stability: potential implications for plaque rupture. Am. J. Physiol. Heart Circ. Physiol. 303, 619–628.

Maldonado, N., Kelly-Arnold, A., Cardoso, L., Weinbaum, S., 2013. The explosive growth of small voids in vulnerable cap rupture; cavitation and interfacial debonding. J. Biomech. 46, 396–401.

Maldonado, N., Kelly-Arnold, A., Laudier, D., Weinbaum, S., Cardoso, L., 2015. Imaging and analysis of microcalcifications and lipid/necrotic core calcification in fibrous cap atheroma. Int. J. Cardiovasc. Imag. 31, 1079.

Melike, B., David, P., Ja St, C., William, T.A., 2018. Clinical significance and applications of D-Ribose in cardiovascular disease. International Archives of Cardiovascular Diseases 2. https://doi.org/10.23937/iacvd-2017/1710013.

Milzi, A., Lemma, E.D., Dettori, R., Burgmaier, K., Marx, N., Reith, S., Burgmaier, M., 2021. Coronary plaque composition influences biomechanical stress and predicts plaque rupture in a morpho-mechanic OCT analysis. eLife 10. https://doi.org/10.7554/eLife.64020.

Moss, A.J., et al., 2020. Ex vivo 18F-fluoride uptake and hydroxyapatite deposition in human coronary atherosclerosis. Sci. Rep. 10, 1–9.

Neels, J.G., Gollentz, C., Chinetti, G., 2023. Macrophage death in atherosclerosis: potential role in calcification. Front. Immunol. 14. https://doi.org/10.3389/fimmu.2023.1215612.

New, S.E.P., Aikawa, E., 2013. The role of extracellular vesicles in de novo mineralization: an additional novel mechanism of cardiovascular calcification. Arterioscler. Thromb. Vasc. Biol. 33, 1753.

Ohayon, J., Finet, G., Gharib, A.M., Herzka, D.A., Tracqui, P., Heroux, J., Rioufol, G., Kotys, M.S., Elagha, A., Pettigrew, R.I., 2008. Necrotic core thickness and positive arterial remodeling index: emergent biomechanical factors for evaluating the risk of plaque rupture. Am. J. Physiol. Heart Circ. Physiol. 295, H717–H727. https://doi.org/10.1152/ajpheart.00005.2008.

Otsuka, F., et al., 2014. Has our understanding of calcification in human coronary atherosclerosis progressed? Arterioscler. Thromb. Vasc. Biol. 34, 724–736.

Perrotta, I., Perri, E., 2017. Ultrastructural, elemental and mineralogical analysis of vascular calcification in atherosclerosis. Microsc. Microanal. 23, 1030–1039.

Proudfoot, D., Skepper, J.N., Hegyi, L., Farzaneh-Far, A., Shanahan, C.M., Weissberg, P. L., 2001. The role of apoptosis in the initiation of vascular calcification. Z. Kardiol. 90, III43–III46. https://doi.org/10.1007/s003920170041.

Rambhia, S.H., et al., 2012. Microcalcifications increase coronary vulnerable plaque rupture potential: a patient-based micro-CT fluid-structure interaction study. Ann. Biomed. Eng. 40, 1443–1454.

Schaar, J.A., De Korte, C.L., Mastik, F., Strijder, C., Pasterkamp, G., Boersma, E., Serruys, P.W., Van Der Steen, A.F.W., 2003. Characterizing vulnerable plaque features with intravascular elastography. Circulation 108, 2636–2641. https://doi.org/10.1161/01.CIR.0000097067.96619.1F.

Schindelin, J., Arganda-Carreras, I., Frise, E., Kaynig, V., Longair, M., Pietzsch, T., Preibisch, S., Rueden, C., Saalfeld, S., Schmid, B., Tinevez, J.-Y., White, D.J., Hartenstein, V., Eliceiri, K., Tomancak, P., Cardona, A., 2012. Fiji: an open-source platform for biological-image analysis. Nat. Methods 9, 676–682. https://doi.org/10.1038/nmeth.2019.

SCOT-HEART Investigators, 2018. Coronary CT angiography and 5-Year risk of myocardial infarction. N. Engl. J. Med. 379, 924–933. https://doi.org/10.1056/NEJMoa1805971.

Stöger, J.L., et al., 2012. Distribution of macrophage polarization markers in human atherosclerosis. Atherosclerosis 225, 461–468.

Torun, S.G., Munoz, P.D.M., Crielaard, H., Verhagen, H.J.M., Kremers, G.-J., van der Steen, A.F.W., Akyildiz, A.C., 2023. Local characterization of collagen architecture and mechanical failure properties of fibrous plaque tissue of atherosclerotic human carotid arteries. Acta Biomater. 164. https://doi.org/10.1016/j.actbio.2023.04.022.

Vengrenyuk, Y., et al., 2006. A hypothesis for vulnerable plaque rupture due to stress-induced debonding around cellular microcalcifications in thin fibrous caps. Proc. Natl. Acad. Sci. U. S. A. 103, 14678–14683.

Virmani, R., Burke, A.P., Farb, A., Kolodgie, F.D., 2006. Pathology of the vulnerable plaque. J. Am. Coll. Cardiol. 47, C13–C18.

Visseren, F., Mach, F., Smulders, Y.M., Carballo, D., Koskinas, K.C., Bäck, Maria, Benetos, A., Biffi, A., Boavida, J.M., Capodanno, D., Cosyns, B., Crawford, C.A., Davos, C.H., Desormais, I., Di Angelantonio, E., Duran, O.H.F., Halvorsen, S., Richard Hobbs, F.D., Hollander, M., Jankowska, E.A., Michal, M., Sacco, S., Sattar, N., Tokgozoglu, L., Tonstad, S., Tsioufis, K.P., van Dis, I., van Gelder, I.C., Wanner, C., Williams, B., De Backer, G., Regitz-Zagrosek, V., Aamodt, A.H., Abdelhamid, M., Aboyans, V., Albus, C., Asteggiano, R., Bäck, Magnus, Borger, M.A., Brotons, C., Celutkiene, J., Cifkova, R., Cikes, M., Cosentino, F., Dagres, N., De Backer, T., De Bacquer, D., Delgado, V., Ruijter, H. Den, Dendale, P., Drexel, H., Falk, V., Fauchier, L., Ference, B.A., Ferrières, J., Ferrini, M., Fisher, M., Fliser, D., Fras, Z., Gaita, D., Giampaoli, S., Gielen, S., Graham, I., Jennings, C., Jorgensen, T., Kautzky-Willer, A., Kavousi, M., Koenig, W., Konradi, A., Kotecha, D., Landmesser, U., Lettino, M., Lewis, B.S., Linhart, A., Løchen, M.L., Makrilakis, K., Mancia, G., Marques-Vidal, P., McEvoy, J.W., McGreavy, P., Merkely, B., Neubeck, L., Nielsen, J.C., Perk, J., Petersen, S.E., Petronio, A.S., Piepoli, M., Pogosova, N.G., Prescott, E.I.B., Ray, K.K., Reiner, Z., Richter, D.J., Rydén, L., Shlyakhto, E., Sitges, M., Sousa-Uva, M., Sudano, I., Tiberi, M., Touyz, R.M., Ungar, A., Monique Verschuren, W.M., Wiklund, O., Wood, D., Zamorano, J.L., 2021. 2021 ESC Guidelines on cardiovascular disease prevention in clinical practice. Eur. Heart J. https://doi.org/10.1093/eurheartj/ehab484.

Walsh, M.T., Cunnane, E.M., Mulvihill, J.J., Akyildiz, A.C., Gijsen, F.J.H., Holzapfel, G. A., 2014. Uniaxial tensile testing approaches for characterisation of atherosclerotic plaques. J. Biomech. 47, 793–804. https://doi.org/10.1016/j.jbiomech.2014.01.017.

Wenk, J.F., 2011. Numerical modeling of stress in stenotic arteries with microcalcifications: a parameter sensitivity Study. J. Biomech. Eng. 133. https://doi.org/10.1115/1.4003128.

Wenk, J.F., Papadopoulos, P., Zohdi, T.I., 2010. Numerical modeling of stress in stenotic arteries with microcalcifications: a micromechanical approximation. J. Biomech. Eng. 132, 14503.

Wissing, T.B., Van Der Heiden, K., Serra, S.M., Smits, A.I.P.M., Bouten, C.V.C., Gijsen, F. J.H., 2022. Tissue-engineered collagenous fibrous cap models to systematically elucidate atherosclerotic plaque rupture. https://doi.org/10.1101/2021.07.20.451997.

Wong, K.K., Thavornpattanapong, P., Cheung, S.C., Sun, Z., Tu, J., 2012. Effect of calcification on the mechanical stability of plaque based on a three-dimensional

carotid bifurcation model. BMC Cardiovasc. Disord. 12, 7. https://doi.org/10.1186/1471-2261-12-7.

Zadpoor, A.A., 2015. Mechanics of biological tissues and biomaterials: current trends. Materials. https://doi.org/10.3390/ma8074505.

Zhou, Y., Song, Y., Liu, Z., Li, W., Guo, Y., Matkovic, L.A., Yang, X., Ma, R., Wan, M., Ruan, L., Zhang, H., 2022. The viscoelastic characteristics of in-vitro carotid plaque by Kelvin-Voigt fractional derivative modeling. J. Biomech. 141, 111210. https://doi.org/10.1016/j.jbiomech.2022.111210.